The Development of LOX-based Magnetic Fluid Technology and its Impact on Small Satellites

Jeffrey C. Boulware
PhD Candidate, Utah State University
Heng Ban
Faculty Advisor, Utah State University

A magnetic fluid system could potentially replace mechanically moving parts in a satellite as a means of increasing system reliability and mission lifetime, but rather than a standard ferrofluid with magnetic particles, liquid oxygen (LOX) may be a more adequate working fluid. As a pure paramagnetic cryogen, LOX is already heavily used in space, but still requires basic research before being integrated into system development. The objectives of the research conducted were to verify LOX as a magnetic working fluid through experiment and establish a theoretical model to describe its behavior. This paper presents the theoretical, experimental, and numerical results of a slug of LOX being pulsed by a 1.1 T solenoid in a quartz tube with an inner diameter of 1.9 mm. The slug oscillated about the solenoid at 6-8 Hz, producing a pressure change of up to 1.2 kPa. System efficiency based on the Mason number was also studied for various geometric setups, and, using a one-dimensional, finite-differenced model in Matlab 2008a, the numerical analyses confirmed the theoretical model. The research provides groundwork for future applied studies using Comsol Multiphysics 3.5a with complex designs.

Introduction

A magnetic fluid actuator using liquid oxygen (LOX) could potentially replace the moving parts in a small satellite which would, therefore, decrease dynamic loads during launch, mission-interfering vibrations, and overall risk of failure. But, while magnetic fluid technology has been used on Earth for decades, application to the cryogenic realm has not been significantly studied.

Conventional magnetic fluids are composed of a carrier fluid and a colloidal suspension of magnetic particles and are referred to as "ferrofluids." Because of the thermal properties of the carrier fluid, typically water, oil, or a hydrocarbon, ferrofluids freeze in the cold temperatures of space. LOX, on the other hand, is a pure paramagnetic fluid and is already used for life support, thermal management, and propulsion. While it seems to be a potential solution for cryogenic magnetic fluid technology, insufficient research exists on its quantitative experimental behavior; thus, the objective of the current study was to establish the viability of LOX as a working fluid through experiments and a theoretical model. By pulsing a magnetic field about a small slug of LOX in a tube, fluid motion occurs due to the magnetic body force. Comparison of the applied power and pressure change generated by slug motion indicates system capability and potential to replace a mechanical subsystem in a small satellite.

Background

Satellite design is a continually evolving process which adapts to enable wider ranges of missions and capabilities, but requires innovation and diversity of basic operating mechanisms to sustain development demand. Of the over 1500 satellites from 0.1–100 kg that have launched since Sputnik[1], Hecht reports that 24.8% of the failures that occurred were design related[2]. Mechanical failures are among the most notorious due to their low fault tolerance and are apparent in all classes of satellites, as reviewed by

Harland[3]. Early tape recorder failures from spinning parts were experienced in small and large spacecraft such as the Ariel 3, Shinsei, Prospero, Spot 1, Compton Gamma Ray Observatory, and Galileo missions. Some failures, such as antenna or boom deployment, are recoverable, but still bear a considerable cost to find a solution, such as in the Voyager II, Anik E2, UoSat 1, and JERS 1 missions. Modern satellites undergo rigorous testing and use highly reliable parts, but an alternate design solution may be to eliminate the moving parts altogether.

Systems with No Moving Parts

Replacing moving parts requires using non-mechanical forces to generate motion or fluid compression. Bhatia provides an excellent review in the area of heat transfer[4], where, even when fully functioning, mechanically moving parts can hamper satellite operations. He showed that, while the technologies perform well in their roles, each has certain limitations on their applicability. Sorption coolers use chemical or physical adsorption reliably, but dependence on a cryostat limits their lifetime. Heat pipes use capillarity to regulate temperature but cannot generate high pressures or heat fluxes. Dilution refrigerators and thermosiphons are gravity-driven mechanisms and, thus, have difficulty finding application in space. Pulse tubes have performed very well transferring heat with acoustic forces and could potentially be superseded by more advanced thermoacoustic engines[5], but are restricted by geometry due to their method of operation. Vuilleumier cycles are designed to replace mechanical compressors with thermal ones, but have low efficiency. Adiabatic demagnetization refrigerators are responsible for generating the lowest artificial temperatures ever by using the magnetocaloric effect but are still in development for space use. In summary, innovative designs have attempted to use chemical, capillary, gravitational, acoustic, thermal, and magnetic forces to replace mechanically moving Stirling cycle compressors. A magnetically driven mechanism can be particularly useful and robust since the field can be adjusted by an electrically controlled solenoid. The solenoid could then be coupled with a magnetic fluid to create a system with no moving parts similar to that used terrestrially for decades. Although they are intended as the application, small satellites could be useful in testing prototype models through advanced technology demonstrator platforms, such as ESA's Proba or JAXA's INDEX.

Magnetic Fluids

As mentioned, ferrofluids consist of a colloidal suspension of magnetic particles within a carrier fluid such as water, oil, or a hydrocarbon. Since developed by NASA in the 1960s, ferrofluids have led to new designs for pumps[6-11], valves[12], actuators[13], heat pipes[14-15], and even optical tuners[16]. Beyond the thermal limitation of ferrofluids, the presence of particles and their surfactants complicates analyses, mainly due to agglomeration and nonhomogeneity.

Oxygen obtains its paramagnetic susceptibility from its molecular structure and has the bulk effect of being attracted to a magnetic field. This is in contrast to diamagnetic materials, which repel a magnetic field, and ferromagnetic materials, which create their own field. At room temperature, the susceptibility of LOX is nearly negligible but increases as temperature decreases due to the phenomenon, Curie's Law. Furthermore, once oxygen condenses into a liquid at 90 K and 1 atm, its susceptibility per volume is greatly enhanced.

Currently, not much demand exists for low-temperature magnetic fluid systems on Earth, so LOX has been overlooked regarding its use as a magnetic working fluid. For use in space, however, the notion of a pure, paramagnetic cryogen presents a potential solution to developing such technology. Unfortunately, research on LOX as a magnetic working fluid is very limited. Catherall[17] and Hilton[18] investigated the magneto-Archimedes levitation of LOX to determine its use in mineral separation, but did not consider it as a working fluid in an actuator. Catherall also studied its surface instabilities[19] under an inhomogenous field but did not generate a bulk movement of the liquid. Youngquist performed experiments which quantitatively measured the magnetohydrodynamic characteristics of LOX[20], but

it was mainly a benchmark study. While using a solenoid to pulse a magnetic field on one end of a column of LOX in an open-ended U-tube, he measured the displacement of the other end and correlated the results to a numerical model. This study was a valuable first step, but requires an evolution in its goals to achieve progress.

Goals and Objectives

The authors performed research intended to advance the basic science to a higher technology readiness level by developing more demanding goals and objectives. Overall goals for the project were as follows:

1) **Obtain a fundamental understanding of cryogenic magnetohydrodynamics.**
   - *Cryogenics and magnetohydrodynamics are individually well understood but have not been heavily researched in combination.*
2) **Determine the feasibility of a magnetic fluid system with no moving parts.**
   - *A thorough analysis of the industrial impact and optimal methods for integration is required for advanced subsystem development.*
3) **Develop a theoretical model to describe the phenomenon.**
   - *To strengthen the fundamental understanding, a mathematical base is required for all experimentation and analyses.*

Furthermore, specific objectives can be attained which support and initiate the overall goals. These specific objectives are as follows:

1) **Displace a LOX slug using magnetic fields.**
   - *Experimentally accomplishing this would quantify the potential of a LOX-based magnetic fluid system.*
2) **Detect the displacement through pressure.**
   - *Innovative measuring techniques will be required to study how LOX behaves in a magnetic field.*
3) **Simulate the dynamics numerically.**
   - *A verified numerical algorithm can quantify LOX performance outside the scope of laboratory testing.*
4) **Perform parametric studies to examine efficiency optimization methods.**
   - *Information on the sensitivity to uncertainties and geometric variance will help to estimate the potential capability of an optimized system.*

The objectives will prove the viability of LOX as a working fluid and lead the way to advanced, applied research. To accomplish these objectives, a theoretical model was developed and an experimental apparatus was designed. The model and experiment were compared using a numerical simulation written in Matlab and have formed the foundation of the overall goals.

Experiment Description

To better represent a real system, the authors chose to experiment on a slug of LOX rather than a column as in Youngquists's experiments. Magnetic pressure on a slug is maximized when one edge is in the center of the solenoid and the other is in a negligible field. While this is achievable with a long column, a smaller slug is nearly as effective. Figure 1 shows that the magnetic flux density of a 0.6 cm (0.25 in) solenoid drops to 5% of its maximum value of 1.1 T at a distance 1.75 cm from the center of the solenoid (Youngquist's column of LOX totaled 36 cm). This benchmark differs depending on solenoid geometry, applied current, and wire spacing, but the example shows that a slug could achieve nearly the same magnetic pressure with a much smaller mass and length. Eliminating mass and length reduces inertia and shear, which would otherwise retard slug motion.

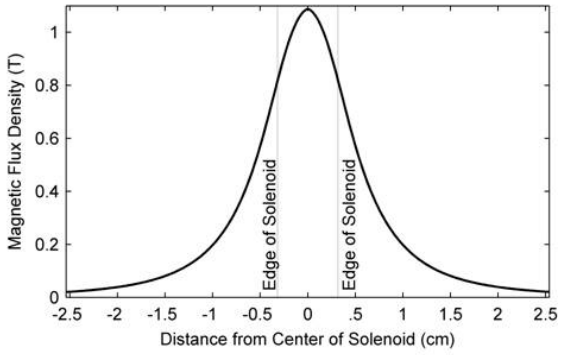

Figure 1. Magnetic flux density along the axis of a solenoid.

A schematic illustrating the basic operations can be seen in Figure 2. The LOX slug began offset from

the solenoid and separated two closed volumes, termed as "upstream" and "downstream." The surrounding gas in the closed volumes was helium, which boils at 4 K and does not react with oxygen. When power was switched to the solenoid, the current induced a magnetic field, and the LOX slug was pulled to the center by a magnetic body force. Figure 2 shows the slug moving towards the upstream section, causing a compression of the upstream volume, V_{US}, and an expansion of the downstream volume, V_{DS}. The displacement causes the upstream pressure, P_{US}, to increase and the downstream pressure, P_{DS}, to decrease. Because the displacement did not cause a significant change in temperature of the helium and the amounts of closed volumes were known, an isothermal ideal gas assumption could be used to translate the change in pressure to a change in displacement.

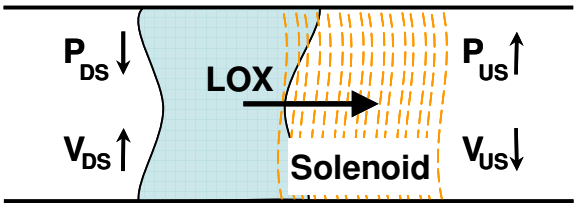

Figure 2. Experimental principle of measuring slug displacement through pressure changes.

To prevent vaporization of the LOX slug, the entire apparatus was submerged in a liquid nitrogen tub at 77 K. As seen in the photograph in Figure 3, the oxygen and helium were introduced to the system at room temperature. Once the system was closed and submerged in the liquid nitrogen tub, the oxygen gas condensed into droplets and fell into the horizontal section of the plumbing. From there, a magnetic wand was used to drag portions of the LOX into a transparent quartz tube with an inner diameter of 1.9 mm. Two different configurations used downstream volumes of 1.8 cm^3 and 5.9 cm^3 for different solenoid sizes, but the upstream volume remained constant at 337 cm^3. Because the downstream volume was significantly less than the upstream volume in both cases, the data from the downstream pressure sensor were used for comparison. The operating pressure was maintained between 100-135 kPa for safety, and the runtime was limited to 0.25 seconds to reduce resistance heating in the solenoids. The LOX slug formed a concave meniscus with edges measureable within 0.8 mm resolution via notches on the quartz tube. While the process allowed for precise measurement of the slug length, an unknown amount of LOX remained in the steel sections. The mass of LOX that could not be seen was dubbed the hidden slug length and could be precisely calculated through the frequency of the pressure oscillations.

The solenoids were powered by a Hewlett-Packard 6268B 900 W DC power supply with an upper limit of 30 V or 30 A. The capability of the power supply was optimized by sizing the solenoids to a resistance of 1 Ω when in the 77 K liquid nitrogen tub. With a known coefficient of temperature resistance of 0.0039 for copper, the corresponding resistance when at room temperature was 6.34 Ω. As mentioned, two solenoid sizes were tested, each with a different gauge wire. Properties of each solenoid are shown in Table 1. Because Solenoid A was physically larger than Solenoid B, it used the 5.9 cm^3 downstream volume and Solenoid B used the 1.8 cm^3 downstream volume.

Table 1. Solenoid specifications.

	Solenoid A	Solenoid B
Wire Gauge:	24	30
Radial Turns:	25	22
Axial Turns:	40	22
Length:	25.6 mm	6.8 mm
ID:	6.3 mm	6.3 mm
OD:	35.1 mm	21.3 mm
Mass:	128.4 g	11.1 g
B_{max}:	1.17 T	1.00 T

Kulite CT-375 analog pressure sensors located upstream and downstream of the slug in the test section were sampled at 5 kHz using a Measurement Computing PCIM-DAS1602/16 A/D card driven by Matlab with Simulink and xPC Target. The sensors had a combined uncertainty of 0.17 kPa from the effects of nonlinearity, hysteresis, 16-bit analog-to-digital conversion errors, and repeatability. Because the changes in the upstream and downstream pressures were the desired output, the absolute

pressure and the measurement uncertainty were not influencing factors. The noise in the raw data was reduced by using a Chebyshev Type II lowpass filter, which was set to 0 dB at 45 Hz and -40 dB at 50 Hz. The filtered, downstream pressure data were compared to the theoretical model implemented in Matlab.

Theoretical Model

For the current study, Rosensweig[21] provides a thorough analysis of the governing equations to describe the magnetic fluid dynamics. The bulk motion of the fluid can be described by the Navier-Stokes equations with an additional term for the magnetic force, also known as the Kelvin force. The Kelvin force density, $\boldsymbol{f_m}$, can be found through the divergence of the Maxwell stress tensor as a function of the permeability of free space μ_o, the magnetization vector **M**, and magnetic field **H** as

$$\boldsymbol{f}_m = \mu_0 (\mathbf{M} \cdot \nabla)\mathbf{H} . \quad (1)$$

In the linear portion of the Langevin function, volumetric magnetic susceptibility, χ, is the ratio of the magnetization vector to the applied field vector, χ = **M** / **H**. By substituting for **M**, using the vector identity, **H**·∇**H** = ∇(**H**·**H**)/2 - **H**×(∇×**H**), and noting that Ampere's Law cancels out the curl of the applied field, Eq. (1) can be reduced to

$$\boldsymbol{f}_m = \mu_0 \chi \nabla \mathbf{H}^2 / 2 . \quad (2)$$

With a constant temperature, the relative permeability, μ, also remains constant. The relative permeability is the ratio between the magnetic flux density, **B**, and applied magnetic fields, μ = **B** / **H**, which can also expressed in terms of volumetric susceptibility, $\mu = \mu_o(1+\chi)$.

Given these relations, the Kelvin force density is

$$\boldsymbol{f}_m = \frac{1}{2\mu_0} \frac{\chi}{(1+\chi)^2} \nabla \mathbf{B}^2 , \quad (3)$$

and the force in the axial direction is

$$f_{m,x} = \frac{1}{2\mu_0} \frac{\chi}{(1+\chi)^2} \frac{d}{dx} B_x^{\,2} ; \quad (4)$$

where the subscript x denotes the axial direction.

The differential term considers the ends of the slug, and when Eq. (4) is integrated over the entire volume with a one-dimensional approximation, the force due to magnetism in the axial direction, F_M, is

$$F_M = \frac{\pi a^2}{2\mu_0} \frac{\chi}{(1+\chi)^2} (B_{x,US}^{\,2} - B_{x,DS}^{\,2}) ; \quad (5)$$

where a is the tube radius and the subscripts US and

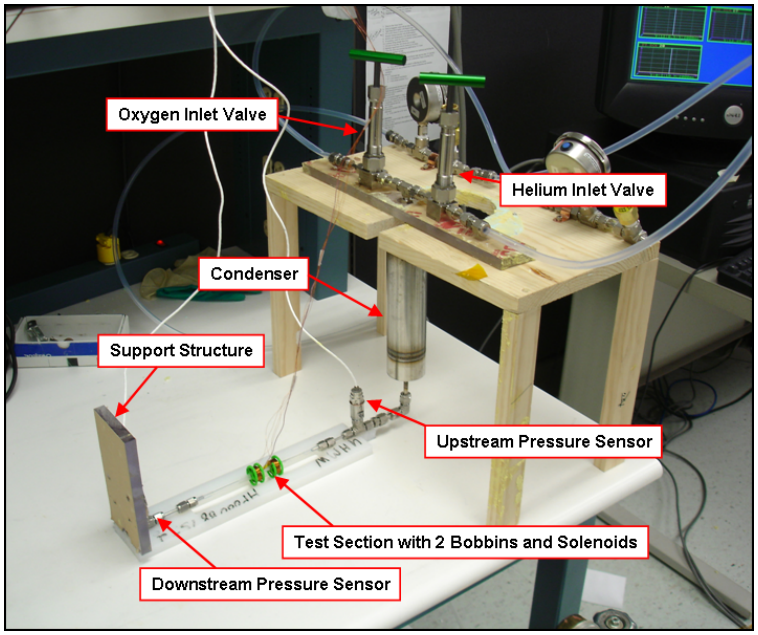

Figure 3. Photograph of test apparatus filled at room temperature.

DS denote the upstream and downstream directions. The magnetic flux density generated by each loop of the solenoid can be found through the Biot-Savart Law and then summed to determine the entire magnetic flux density for the whole solenoid.

Damping on the slug occurs due to its combined oscillatory motion, finite slug length, and magnetoviscous effects. To account for these combined factors, the wall shear stress was calculated using an empirically found damping factor, ζ, and the classic relation for laminar wall shear stress in Hagen-Poiseuille flow. The force due to damping, F_D, was calculated as

$$F_D = 8\pi(L + L_{hidden})\dot{x}\zeta\eta \; ; \qquad (6)$$

where η is the nonmagnetized dynamic viscosity of LOX, L is the visible length of the slug, L_{hidden} is the hidden length of the slug in the steel sections, and $\dot{x}$ is the velocity of the slug in the axial direction. Only the visible slug length is effected by the magnetic field, but both sections must be considered for mass and damping.

The pressure force, F_P, results from the differential pressure on either side of the slug as

$$F_P = \pi a^2 \Delta p \; . \qquad (7)$$

where Δp denotes the pressure differential across the slug. The change in pressure results from the compression and expansion of closed volumes on either side of the slug.

The full equation of motion for the LOX slug is a combination of the pressure, magnetic, and damping forces as,

$$\begin{aligned} m\ddot{x} = {} & \pi a^2 \Delta p \\ & + \frac{\pi a^2}{2\mu_0} \frac{\chi}{(1+\chi)^2} (B_{x,US}{}^2 - B_{x,DS}{}^2) ; \\ & + 8\pi(L + L_{hidden})\dot{x}\zeta\eta \end{aligned} \qquad (8)$$

where m is the total mass of LOX and $\ddot{x}$ is the acceleration. Surface tension, instabilities, and breakdown of the slug are not accounted for in the one-dimensional assumption of an incompressible, finite-length slug. For the experiment, the radius of the slug must be small enough so that surface tension can hold it in place when nonmagnetized, but large enough so that during the pulse, the capillary effects can be considered negligible. Initial calculations had shown that force due to capillarity was approximately 1/50th of the other forces and Bashtovoi[22] has shown that capillary effects are reduced under a magnetic field. Gravity was also ignored because the tube was oriented horizontally.

To apply the theoretical model, the governing equation of motion for the one-dimensional dynamics of the liquid slug, Eq. (8), was discretized and solved numerically with initial conditions from the experiment. The numerical simulation was written in Matlab v7.6.0 (R2008a) on a 2.4GHz Pentium 4 processor with 2GB of RAM. The dynamics were typically solved in less than 2 seconds, allowing for a thorough optimization of system variables through a regression analysis. For a particular test run, the regression analysis calculated the damping factor and hidden slug length which resulted in the lowest root mean square deviation (RMSD) of the absolute error from the experiment. The regression analysis was also able to find an optimal slug length that generated the greatest pressure change for a particular solenoid.

Fluid properties for LOX were taken from the CRC Handbook of Chemistry and Physics[23], and studies by Hilton[24] indicated that the pressure fluctuations would not significantly affect those values.

Results and Discussion

The authors completed the aforementioned objectives and published the results in a series of articles[25-27]. Key findings from the studies are the maximum attainable pressure change in the downstream section, uncertainty determination from the numerical model, and geometric variance of the test parameters. Figure 4 shows an experimental run versus the numerical simulation and was the basis of the analyses. A 0.25 s pulse caused an oscillation of a 1.3 cm slug which had one edge initially in the center of the solenoid. The system pressure was about 131.2 kPa when power was switched to the solenoid at 0.01 s. The downstream pressure fluctuated at

approximately 7 Hz, generating a maximum pressure change of 1.2 kPa at about 0.06 s after the pulse began. The regression analysis found that a hidden slug length of 14.5 cm and a damping factor of 6.08 resulted in the lowest RMSD of the absolute error at 30.6 Pa. The green line in Figure 4 shows the accuracy of the Matlab simulation.

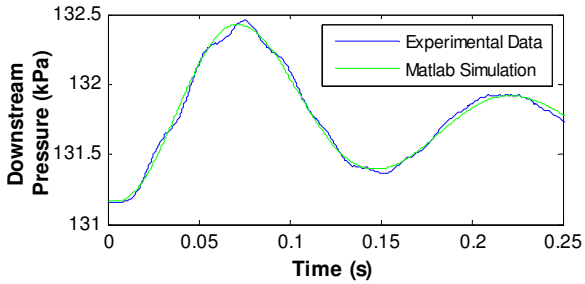

Figure 4. Experimental and simulated pressure oscillations for a 1.3 cm slug.

To perform the parametric studies mentioned in the third objective, several hundred runs similar to Figure 4 were conducted. Each oscillated at about 6-8 Hz with amplitudes relative to the initial conditions and applied current.

Maximum Attainable Pressure Change

In Figure 4, the maximum pressure change was approximately 1.2 kPa at about 0.07 s. One edge of the 1.3 cm slug in the center of the solenoid correlates to an initial center displacement of 0.65 cm between the slug and solenoid. As the initial center displacement varied, a trend was apparent in the maximum pressure change attainable in the downstream end. Increasing the offset of the slug from the solenoid resulted in a higher pressure change symmetrically for compression and expansion, as shown in Figure 5 for various slug lengths. Each of the tests in Figure 5 used Solenoid B, which was calculated to have an optimal slug length of ~1.3 cm from the regression analysis. In Figure 5, the 1.3 cm slug length seemed to generate the greatest magnitude of pressure change, thereby verifying the regression analysis.

Each of the data points in Figure 5 represents a run conducted in which the slug maintained its form and did not break down. If the initial position was too far from the solenoid, the displacement of the slug attempted to generate a pressure force greater than the magnetic force. Stationary experiments with a ferrofluid by Perry[28] verified the theoretical prediction that the pressure force could not exceed the maximum magnetic capability of the solenoid. In Perry's case, the stationary experiments induced a hydrostatic breakdown, whereas, for the current study, the breakdown was during dynamic motion and occurred slightly earlier than the static equations predicted. A probabilistic method to predict risk of failure should be used to predict hydrodynamic breakdown, as it is likely due to a combination of the uneven force distribution along the slug, pressure differential about the slug, gravity, and low surface tension of LOX. For higher speed tests, the rapid oscillations may also induce turbulent internal flow dynamics that cause the slug to break down.

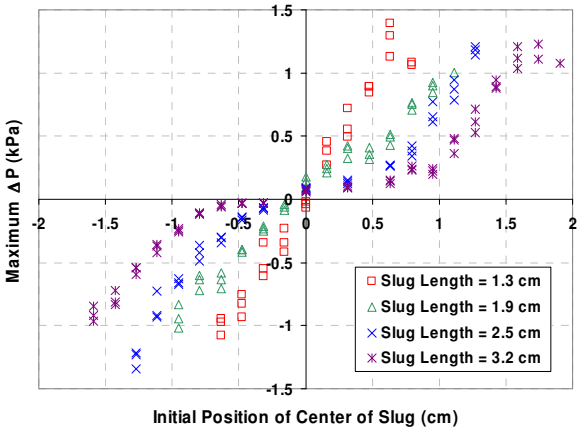

Figure 5. Maximum pressure change for various slug lengths using Solenoid B.

The runs in Figure 5 maximized the capability of the 900 W power supply. For satellite applications, however, it is essential to consider a low power system. Figure 6 shows the maximum pressure change versus current for three slug lengths. Because the Biot-Savart Law denotes a linear relationship between applied current and magnetic flux density, Eq. (5) indicates that the trend in Figure 6 should be quadratic; instead, it appears linear. This is likely due to resistance heating and the limited heat capacity of the solenoid. As the solenoid temperature increases, it cannot draw as much current and, thus, cannot generate as high a magnetic field. At high current

levels, the solenoid may not stay cool long enough to generate high pressures, even during the 0.25 s pulse.

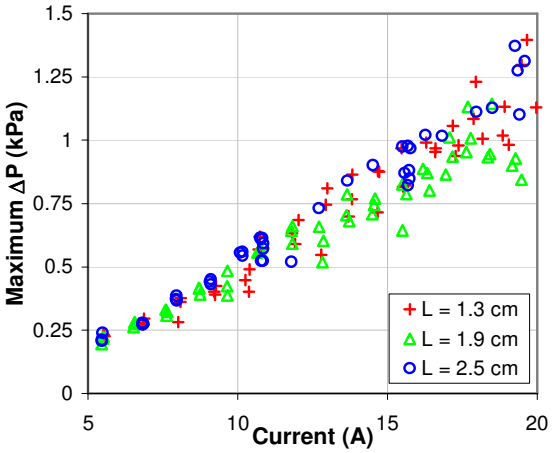

Figure 6. Maximum pressure change for slugs with one edge centered in the solenoid at various currents.

Determining Uncertainty

By extracting the frequency and amplitude of the oscillations in the experimental data, the Matlab model could be used to calculate the hidden slug length, damping factor, and precise initial position of the slug. The authors performed detailed analyses on the uncertainties and found a logarithmic correlation between frequency and hidden slug length and also between amplitude and damping factor, as shown in Figure 7. The initial position of the slug also affected the amplitude; however, unlike the damping factor, it did not cause the mean to decrease over time. Based on the oscillations, these correlations could be used to precisely calculate the hidden slug length, damping factor, and initial position of the slug within the given uncertainty bounds of experimental measurements.

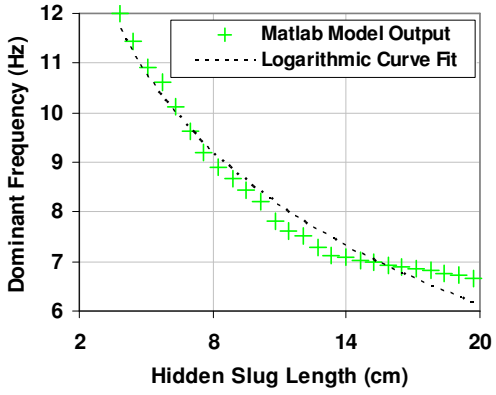

(a)

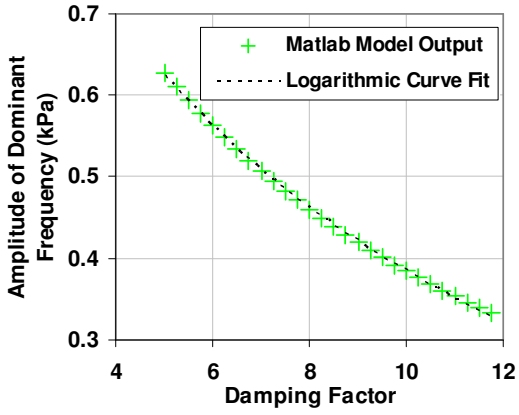

(b)

Figure 7. (a) Hidden slug length vs. frequency and (b) damping factor vs. amplitude.

Geometric Variance

As mentioned, a variety of geometries were tested to determine if an optimal configuration existed. For a particular solenoid, the Matlab model could be used to predict the slug length which would produce the maximum pressure change. In a sense, this optimal length was the result of the highest ratio of initial magnetic pressure to damping and inertia. The authors confirmed the theoretical results by testing three configurations with Solenoids A and B as follows:

- Config. 1: Solenoid A with an optimized slug length of 2.7 cm
- Config. 2: Solenoid B with an optimized slug length of 1.3 cm
- Config. 3: Solenoid B with a nonoptimized slug length of 2.5 cm

Each configuration used the same power source and generated approximately the same pressure change. Treating the pressure change as an indicator of work performed by the fluid would entail approximately the same output per power input for each configuration. However, since fluid damping is detrimental to performance, it could be seen as a form of exergy destruction. Exergy is the potential work of a system and is used to determine its second law efficiency. High damping of the fluid reduces the potential work and, therefore, should be factored in to a measure of the system's second law efficiency. This

measure could be found through a nondimensional number known as the Mason number, the ratio of damping to magnetic forces.

The maximum pressure change was converted to displacement and the time to reach it was used to determine an average initial velocity of the slug, u_i. The initial position of the slug could be used to determine its initial magnetic pressure, $p_{m,i}$, by dividing Eq. (5) by the cross-sectional area. Figure 8 shows $p_{m,i}$ versus u_i for the three configurations. The slope of the linear trend line of each set of data provides an important characteristic of each combination, as it is a component of the Mason number. By modifying Eqs. (5) and (6), the Mason number was defined for the current study as,

$$Ma = \frac{F_D}{F_M} = \frac{8\pi(L + L_{hidden})\zeta\eta u_i}{\pi a^2 p_{m,i}}. \qquad (9)$$

A lower Mason number indicated a more efficient system since less damping would exist for a given magnetic force (achievable through power input). While it seems counter-intuitive that a slower average initial velocity implies a more efficient system, Solenoid A was nearly 4 times longer than Solenoid B; thus the magnitude of velocity was relative. Instead, the Mason number is representative of exergy destruction and should, ideally, be as low as possible.

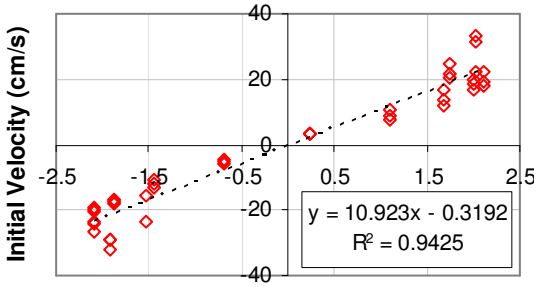

(a)

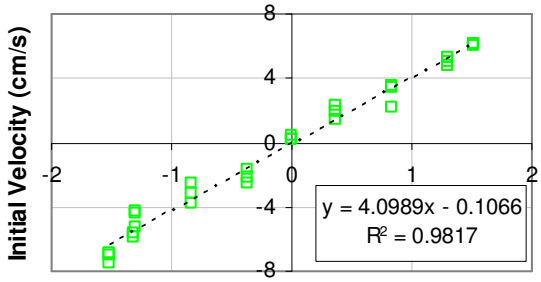

(b)

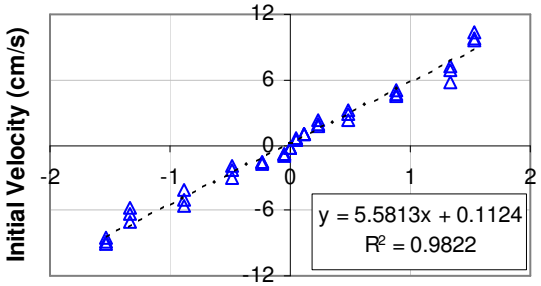

(c)

Figure 8. Average initial velocity versus initial magnetic pressure for (a) Configuration 1, (b) 2, and (c) 3.

The near-linearity of the trend lines indicates that the Mason number is consistent for each configuration. This implies that with a given slug length and profile of the magnetic flux density along the axis of the solenoid, u_i can be calculated through a proportionality constant of $p_{m,i}$. When Eq. (9) is calculated for each run, the average Mason number for each configuration can be found as shown in Table 2, assuming each configuration had an average damping factor of 6 and hidden slug length of 13 cm.

Table 2. Average Mason number

Config.	# of Runs	Avg. Mason #	Std. Dev.
1	41	0.247	$6.62 * 10^{-2}$
2	26	0.091	$2.03 * 10^{-2}$
3	37	0.143	$3.54 * 10^{-2}$

The correlations in Table 2 reveal two methods for improving system efficiency through geometric measures. By optimizing the slug length for a solenoid and by minimizing the overall geometry, less damping can be achieved for a given magnetic force. While this seems particularly beneficial for

small satellites with MEMS technology, it is important to remember that capillarity has not been introduced to the system. Nonetheless, the experiments and analyses performed have verified the theoretical model and are therefore useful to future research and applications.

Future Work

Combining the magnetic, thermal, and fluid phenomena in three dimensions requires a highly sophisticated solver that couples the nonlinear partial differential equations. Comsol Multiphysics 3.5a is currently being used to model the experiments performed to further verify the theoretical model to support the third overall goal. The research will be used to further understand the hydrodynamic breakdown and expand the study to advanced geometries. Figure 9 shows the mesh and magnetic flux density of an axisymmetric model around the test section.

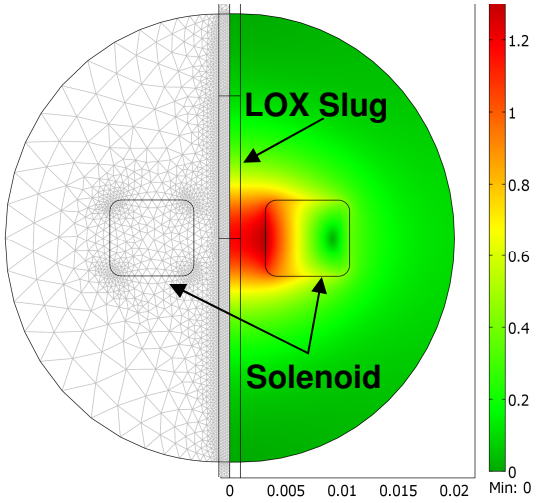

Figure 9. Axisymmetric mesh of the test section and magnetic flux density profile using Comsol Multiphysics 3.5a.

Conclusions

The case for a LOX-based magnetic fluid system to replace mechanically moving parts in a satellite system has been argued. The experiment alone satisfied the first two objectives by confirming the potential of a LOX-based magnetic fluid system through innovative measuring techniques. The experiment and numerical simulation also verified the theoretical model, thus satisfying the third objective. The fourth objective was satisfied through the parametric studies which examined the maximum pressure change attainable, effect of uncertainty, and geometric variance. Accomplishing the objectives aids the overall goals by establishing the following conclusions:

- an optimal slug size for a specific geometry exists that maximizes the attainable pressure change for a given power source;
- a low power system may perform more efficiently due to less resistance heating in the solenoid;
- unknown portions of LOX in the fluid system and undetermined physical phenomena can be empirically calculated through the theoretical model;
- an optimized slug and solenoid configuration will result in a more efficient system in terms of work performed by the fluid per damping;
- reducing the physical scale of the experiment increases its efficiency, assuming capillarity is still negligible.

The conclusions of this research support the overall goals in aiding the design of a LOX-based magnetic fluid system with no moving parts for small satellite applications.

Acknowledgments

The authors wish to acknowledge the assistance of Dr. Scott Jensen, Dr. Steve Wassom, Dr. Bob Anderson, Dr. Clair Batty, Dr. Steve Hansen, Ms. Gayle Bowen, and Dr. Doran Baker for their help in various aspects of this project.

This material is based on the research sponsored by the Air Force Research Laboratory, under agreement number FA9550-08-1-0018. The U.S. Government is authorized to reproduce and distribute reprints for Governmental purposes notwithstanding any copyright notation thereon. The views and conclusions contained herein are those of the authors and should not be interpreted as necessarily representing the official policies or endorsements,

either expressed or implied, of the Air Force Research Laboratory or the U.S. Government.

References

1. Janson, S. W., "The History of Small Satellites," *Small Satellites: Past, Present, and Future*, edited by H. Helvajian and S. W. Janson, The Aerospace Press, AIAA, Reston, VA, 2008, pp. 47-49.
2. Hecht, H., "Reliability During Space Mission Concept Exploration," *Space Mission Analysis and Design*, edited by J. R. Wertz and W. J. Larson, Kluwer Academic Publishers, Dordrecht, 1991, pp. 640-656.
3. Harland, D. M., and Lorenz, R. D., *Space Systems Failures*, Praxis Publishing, Chichester, UK, 2005, pp. 295-304.
4. Bhatia, R. S., "Review of Spacecraft Cryogenic Coolers," *J Spacecraft and Rockets*, Vol. 39, No. 3, 2002, pp. 329-346.
5. Gardner D. L. and Swift, G. W., "A Cascade Thermoacoustic Engine," *J. Acoust. Soc. Am.*, Vol. 114, No. 4, 2003, pp. 1905-1919.
6. Park, G. S., and Seo, K., "A Study on the Pumping Forces of the Magnetic Fluid Linear Pump," *IEEE Trans on Magn*, Vol. 39, 2003, pp. 1468-1471.
7. Park, G. S., and Seo, K., "New Design of the Magnetic Fluid Linear Pump to Reduce the Discontinuities of the Pumping Forces," *IEEE Trans on Magn*, Vol. 40, 2004, pp. 916-919.
8. Seo, K. and Park, G. S., "A Research on the Pumping Forces in the Magnetic Fluid Linear Pump," *IEEE Trans on Magn*, Vol. 41, No. 5, 2005, pp. 1580-1583.
9. Hatch, A. and Kamholz, A. E., "A Ferrofluidic Magnetic Micropump," *J. of Microelectromech. Syst.*, Vol. 10, 2001, pp. 215-221.
10. Moghadam, M. E., Shafii, M. B., and Dehkordi, E. A., "Hydromagnetic Micropump and Flow Controller. Part A: Experiments with Nickel Particles Added to the Water," *Exp Therm Fluid Sci*, Vol. 33, No. 6, 2009, pp. 1021-1028.
11. Krauss, R. and Liu, M., "Pumping Fluid by Magnetic Surface Stress," *New J. of Physics*, Vol. 8 No. 18, 2006, pp. 1-11.
12. Goldstein, S. R., Bethesda, MD, U.S. Patent Application for a "Magnetic Fluid Actuated Control Valve, Relief Valve and Pump," No. 4053952, filed 8 Apr. 1977.
13. Kamiyama, S., "A Magnetic Fluid Actuator," *Advanced Robotics*, Vol. 1, No. 2, 1986, pp. 177-185.
14. Ming, Z., Zhongliang, L., Guoyuan, M., and Shuiyuan, C., "The Experimental Study on Flat Plate Heat Pipe of Magnetic Working Fluid," *Exp Therm Fluid Sci*, Vol. 33, No. 7, 2009, pp. 1100-1105.
15. Jeyadevan, B., Koganezawa, H., and Nakatsuka, K., "Performance Evaluation of Citric Ion-Stabilized Magnetic Fluid Heat Pipe," *J Magn Magn Mater*, Vol. 289, 2005, pp. 253-256.
16. Liao, W. and Chen, X., "Tunable Optical Fiber Filters with Magnetic Fluids," *Applied Physics Letters*, Vol. 87, 2005 pp. 1-3.
17. Catherall, A. T., López-Alcaraz, P., Benedict, K. A., King, P. J., and Eaves, L., "Cryogenically Enhanced Magneto-Archimedes Levitation," *New J Phys*, Vol. 7, No. 118, 2005, pp. 1-10.
18. Hilton, D. K., Celik, D., and Van Sciver, S. W., "Subcooled Liquid Oxygen Cryostat for Magneto-Archimedes Particle Separation by Density," *Adv Cryo Eng*, CP985, Vol. 53, AIP, 2008, pp. 1517-1522.
19. Catherall, A. T., Benedict, K. A., King, P. J., and Eaves, L., "Surface Instabilities on Liquid Oxygen in an Inhomogeneous Magnetic Field," *Phys Rev E*, Vol. 68, 2003, pp. 1-3.
20. Youngquist, R. C. and Immer, C. D., "Dynamics of a Finite Liquid Oxygen Column in a Pulsed Magnetic Field," *IEEE Trans. on Magnetic*, Vol. 39, 2003, pp. 2068-2073.
21. Rosensweig, R. E., *Ferrohydrodynamics*, Dover, New York, 1985.

22. Bashtovoi, V., Kuzhir, P., and Reks, A., "Capillary Ascension of Magnetic Fluids," *J Magn Magn Mater*, Vol. 252, 2002, pp. 265-267.
23. Lide D. R. (ed.), *CRC Handbook of Chemistry and Physics*, 89th Edition, CRC Press/Taylor and Francis, Boca Raton, 2009.
24. Hilton, D. K. and Van Sciver, S. W., "Absolute Dynamic Viscosity Measurements of Subcooled Liquid Oxygen from 0.15 MPa to 1.0 MPa," *Cryogenics*, Vol. 48, 2008, pp. 56-60.
25. Boulware, J. C., Ban, H., Jensen, S., and Wassom, S., "Experimental Studies of the Pressures Generated by a Liquid Oxygen Slug in a Magnetic Field," *J Magn Magn Mater*., Vol. 322, 2010, pp. 1752-1757.
26. Boulware, J. C., Ban, H., Jensen, S., and Wassom, S., "Modeling of the Dynamics of a Slug of Liquid Oxygen in a Magnetic Field and Experimental Verification," *Cryogenics*, 2010, doi:10.1016/j.cryogenics.2010.03.004.
27. Boulware, J. C., Ban, H., Jensen, S., and Wassom, S., "Geometric Influence on Liquid Oxygen Magnetohydrodynamics," submitted for publication in *Exp Therm Fluid Sci*.
28. Perry, M. P. and Jones, T. B., "Hydrostatic Loading of Magnetic Liquid Seals," *IEEE Trans. on Magnetics*, Vol. MAG-12, No. 6, 1976, pp. 798-800.